Journal of Solid State Chemistry 182 (2009) 3330–3341

Contents lists available at ScienceDirect

Journal of Solid State Chemistry

journal homepage: www.elsevier.com/locate/jssc

Intercalation of stable organic radicals into layered inorganic host matrices: Preparation and structural characterization of $Cd_{1-x}PS_3$(*meta*MPYNN)$_{2x}$

Wilhelm L. Hemme [a], Wataru Fujita [b], Kunio Awaga [b], Hellmut Eckert [a,*]

[a] Institut für Physikalische Chemie, Westfälische Wilhelms-Universität, Corrensstr. 30, 48149 Münster, Germany
[b] Research Center for Materials Sciences & Department of Chemistry, Nagoya University Furo-cho, Chikusa, Nagoya 464-8602, Japan

ARTICLE INFO

Article history:
Received 17 July 2009
Received in revised form
23 September 2009
Accepted 28 September 2009
Available online 2 October 2009

Keywords:
Intercalation compounds
Nitroxide radicals
Solid state NMR

ABSTRACT

The radical cation 2-(3-*N*-methylpyridinium)-4,4,5,5-tetramethyl-4,5-dihydro-1H-imidazol-1-oxyl-3-*N*-oxide (abbreviated as *m*-MPYNN) is successfully intercalated into the layered host structure $CdPS_3$. The reaction proceeds via an ion exchange reaction from methanol solutions containing the radical iodide salt, leading to materials described by the compositional formula $Cd_{1-x}PS_3$(*meta*MPYNN)$_{2x}$. Detailed characterization of the intercalates by chemical analysis, X-ray powder diffraction, EPR, and NMR spectroscopy indicate that the maximum uptake corresponds to $x=0.20$; attempts to produce higher intercalated materials result in the formation of a side product with inferred composition CdI_4(*meta*MPYNN)$_2$. Magnetic susceptibility measurements indicate CURIE-like behavior for $x=0.13$, while at higher intercalation levels antiferromagnetic coupling is observed. The magnetic properties may be linked to the orientation of the radical ions relative to the host layers, which is also found to depend on x. While for the low-intercalated regime ($x=0.13$) both a transversal intercalation with the N–O director pointing towards the layers, and a longitudinal orientation, with the long axis of the molecule pointing towards the layers are found, at larger x-values only the longitudinal orientation is present. ^{1}H NMR chemical shifts indicate that the orientation greatly influences the molecular spin density distributions. Modern single and double resonance solid state NMR techniques have been introduced successfully to study the structural modifications of the host lattice and the details of the intermolecular guest/host interactions. Specifically the internuclear distance correlations extracted from selectively measured ^{1}H–^{31}P magnetic dipole–dipole couplings via ^{31}P/^{1}H rotational echo double resonance (REDOR) experiments allow important conclusions regarding the orientation of the guest species relative to the inorganic layers.

1. Introduction

Ever since the first reports on bulk ferromagnetism in purely organic compounds based on stable radicals [1,2] such materials have attracted widespread interest from the viewpoints of both fundamental science and applied materials. It was noted that ferromagnetic interactions have been observed particularly frequently in solids based on nitronyl nitroxide radicals and their cation salts [3], and numerous publications have discussed magnetic behavior in relation to the relative orientations of the spin-carrying moieties [3–9]. In this context, a large crystal structure database has been generated [4] by synthesizing many nitronyl nitroxide variants with different ring substituents, presenting a wide variety of magnetic properties. Another way to modify the intermolecular interactions between (and thence the magnetic properties of) nitroxide (and other) radicals is to use them as building blocks in inorganic–organic hybrid materials and/or nanocomposites. Hybrids of this kind can be generated by coordination chemistry [10–12], self-assembly processes on surfaces [13–16] or by topotactic reactions of inorganic solids [17–19]. In the latter approach, the radical species are intercalated as guest molecules or ions into the interlayer space of inorganic layered host structures. The spatial confinement within the interlayer space as well as the intermolecular interactions between the host lattice and the guest species can lead to greatly modified orientations of the spin-carrying moieties and molecules compared to the situation in the molecular crystals, resulting in modified magnetic properties. The most prominent host material in which this objective has been studied is the layered clay compound saponite $\{Na_x[Si_{4-x}Al_xMg_3O_{10}(OH)_2]\cdot nH_2O\}$, where radical intercalation has already been demonstrated [18,19]. Another potentially useful host material for which the inclusion of numerous organic guest species has already been successfully demonstrated, is layered cadmium phosphorus sulfide, $CdPS_3$,

* Corresponding author.
E-mail address: eckerth@uni-muenster.de (H. Eckert).

0022-4596/$ - see front matter © 2009 Elsevier Inc. All rights reserved.
doi:10.1016/j.jssc.2009.09.030

[20–24]. In the present study, this material has been used, for the first time, for the intercalation of a stable organic radical, namely *meta*(*m*)-methylpyridylnitronyl nitroxide. The intercalation reaction can be described by the equation,

$$CdPS_3 + 2x\ meta\text{-MPYNNI} \rightarrow Cd_{1-x}PS_3(meta\text{MPYNN})_{2x} + x\ CdI_2$$

i.e. it proceeds via an exchange of Cd^{2+} ions from the host matrix. We have prepared materials with different degrees of intercalation x and characterized them with respect to their magnetic and structural properties using X-ray powder diffraction, bulk property measurements, and a number of spectroscopic techniques. For the first time, we introduce the use of multinuclear high-resolution solid state nuclear magnetic resonance to monitor the intercalation process. Specifically, high-speed ^{1}H magic-angle spinning (MAS) NMR is used to characterize modifications in the spin density distributions of the radical guest species upon insertion into the host lattice. Furthermore, owing to the presence of the NMR active nuclei ^{31}P and ^{113}Cd the $CdPS_3$ intercalates afford opportunities for characterizing the structural modifications of the host lattice and for probing the guest–host interaction in more detail. To this end, the present contribution introduces various advanced NMR techniques, such as spin-lattice relaxation measurements, rotational echo double resonance (REDOR), homonuclear J-Resolved and heteronuclear correlation (HETCOR) experiments, as new structural probes for these inorganic–organic hybrid materials.

2. Experimental

2.1. Sample preparation and characterization

$CdPS_3$ was prepared by heating stoichiometric amounts of the elements in an evacuated glassy silica ampoule for two weeks at 680 °C [21]. Its phase purity was verified by X-ray powder diffraction and solid state NMR. The bright yellow crystals were ball milled for 1 h in a zirconia mortar and sieved. The nitronyl nitroxide radical ion *meta*-$MPYNN^+$ (Fig. 1) was prepared as the iodide salt according to reported methods [25,26]. Intercalation compound samples were prepared by stirring a methanol solution of *meta*-MPYNNI for 10 days with ball milled $CdPS_3$ at room temperature within an evacuated quartz ampoule. In a typical reaction, 100 mg $CdPS_3$ were stirred in 10 ml of a 83.5 mM radical solution, which means that 0.835 mmol of radical was offered to the host material. This amount of the singly charged radical cation corresponds to the ionic equivalent to the entire Cd^{2+} ion content inside the host lattice ($x=1$, $R=n(\text{rad})/n(CdPS_3)=2$). By varying the concentration R of the radical cations, a series of intercalation compounds with varying radical contents x was prepared. x was quantified by both CHN elemental analysis and EPR spectroscopy (referencing the signal intensity against that of the pure radical standard). As the weight percentage value, wt%, is given by

$$wt\% = \frac{2x\mathrm{M}(m\mathrm{MPYNN})}{\mathrm{M}(CdPS_3) - x\mathrm{M}(\mathrm{Cd}) + 2x\mathrm{M}(m\mathrm{MPYNN})}$$

the intercalation degree x can be calculated from the formula

$$x = \frac{\mathrm{M}(CdPS_3)\cdot wt\%}{\mathrm{M}(\mathrm{Cd})\cdot wt\% + 2\mathrm{M}(\mathrm{mMPYNN})\cdot(1 - wt\%)}$$

where M(*m*MPYNN), $M(CdPS_3)$ and M(Cd) are the molecular masses of the radical cation, the host lattice and cadmium, respectively. The ICP-MS (Inductively Coupled Plasma Mass Spectrometry) measurements of Cd, P and S contents were done by the company Wessling Laboratorien GmbH Altenberge. X-ray diffraction data were measured on a Rigaku Multiflex instrument using a Cu$K\alpha$ source. EPR measurements were conducted at 300 K on a JES-FA200 X-band spectrometer. Magnetic susceptibility measurements were carried out over the temperature range 4–300 K using a Superconducting Quantum Interference Device (SQUID) from Quantum Design.

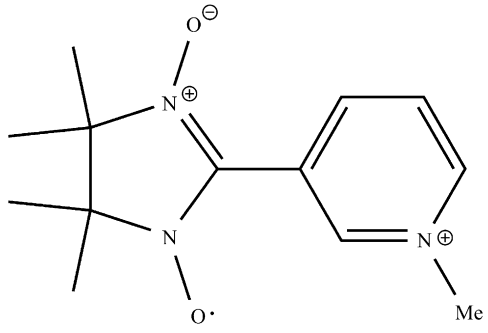

Fig. 1. The radical cation *meta*-MPYNN, 2-(3-*N*-methylpyridinium)-4,4,5,5-tetramethyl-4,5-dihydro-1H-imidazol-1-oxyl-3-*N*-oxide.

2.2. Solid State NMR measurements

^{1}H and ^{31}P solid state NMR spectra were recorded on a Bruker DSX 500 spectrometer equipped with a 2.5 mm MAS NMR probe operated at spinning frequencies between 15 and 35 kHz. Temperature dependent measurements were all carried out at a rotation frequency of 20 kHz and calibrated based on the ^{207}Pb MAS-NMR signal of lead nitrate as described in the literature [27]. Typical 90° pulse lengths and relaxation delays were, respectively, 2 μs, and 0.1–10 s for ^{1}H and 2 μs and 0.1–1000 s for ^{31}P. ^{31}P spin-lattice relaxation times were measured at 202.5 MHz under MAS conditions, using the saturation recovery technique with pulses of 2 μs length. In samples with multiple ^{31}P environments, separate T_1 values for each of the lineshape components could be extracted by manual constrained peak fitting (DMFIT program [28]), using consistent lineshape parameters for the individual components. Chemical shifts are reported relative to tetramethylsilane (^{1}H) and 85% H_3PO_4. $^{31}P\{^{1}H\}$ 2-D heteronuclear correlation (HETCOR) spectra were obtained under the following conditions: 90° pulse length 2 μs, cross-polarization contact time 1 ms, relaxation delay 1–60 s, and spinning frequency 30 kHz. 256 FIDs were recorded with a dwell time of 40 μs in the t_1 dimension. 2-D J-Resolved ^{31}P NMR spectra [29,30] were obtained under similar conditions as the HETCOR data. The time increment in the t_1 dimension was 160 μs with 400 acquired FIDs at a spinning speed of 25 kHz. In addition, heteronuclear magnetic dipole–dipole interactions were probed by $^{1}H/^{31}P$ rotational echo double resonance (REDOR) experiments, using the sequence by Gullion and Schaefer [31] operated under the following conditions: spinning frequency 30 kHz, 90° pulse length 2 μs, length of the ^{31}P inversion pulses 2.5 μs, relaxation delay 1 s. The data were analyzed by approximating the REDOR curves within the initial decay regime ($\Delta S/S_o < 0.2$) by a parabola, yielding average dipolar second moments M_2 quantifying the heteronuclear magnetic dipole–dipole interactions as described in the literature [32,33]. ^{113}Cd MAS NMR spectra were recorded at 66.57 MHz, using a Bruker CXP300 FT-NMR spectrometer equipped with a Bruker 4 mm WVT probe. Typical 90° pulse lengths were 3 μs. 5000–80 000 scans were recorded with a spinning speed of 10 kHz and a delay of 1–60 s. Chemical shifts are reported relative to a 1 M $Cd(NO_3)_2$ solution.

3. Results and discussion

3.1. Radical content

Fig. 2 shows the uptake curve (dependence of radical content in the intercalation compound x on the amount of radical offered in the solution R). The horizontal axis is defined as the molar ratio R ($=n(\text{rad})/n(CdPS_3)$) of the offered radical in the original solution to the $CdPS_3$ host matrix. The ordinate shows the amount x of intercalated radical per formula unit of $CdPS_3$, determined via elemental analysis and EPR peak intensity measurement. Fig. 2 indicates excellent agreement between both analytical methods. There are two distinct regimes. In the low-concentration regime x increases linearly with increasing R up to $x=0.14$, where a plateau value is reached near $R=1$. In the high-concentration regime ($R\sim3$), x increases further and reaches a second plateau value of $x=0.27$.

Table 1 shows the result of ICP-MS measurements on pure $CdPS_3$ and one representative sample of each intercalation regime. The results of the pure host lattice and the low-intercalation regime sample are in good agreement with the predicted elemental formula for a pure material and confirm that the elemental formula of $Cd_{1-x}PS_3(meta\text{MPYNN})_{2x}$ is correct for

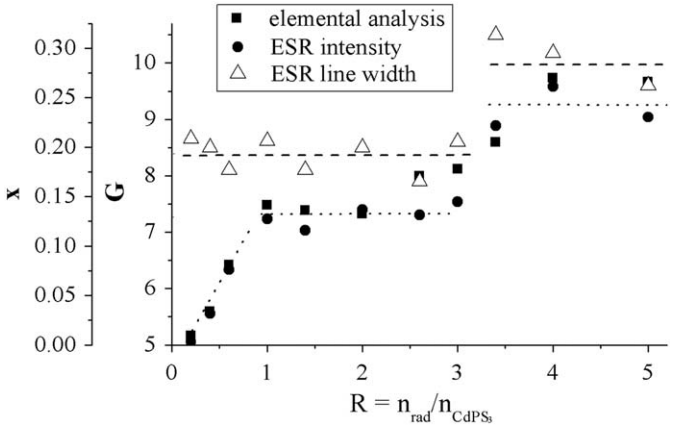

Fig. 2. Uptake curves of *meta*-MPYNN into $CdPS_3$ as determined by elemental analysis and EPR signal intensity measurements. Included is the EPR line width as a function of composition.

Table 1
Overview of elemental analysis and ESR results of the intercalation series $Cd_{1-x}PS_3(meta\text{MPYNN})_{2x}$.

R	Elemental analysis % mass			wt% radical	x (anal.)	x (ESR)	Δ^a (G)
	C	H	N				
0.2	0.78	0.21	0.22	1.76 ± 0.32	**0.01**	0.01	8.7
0.4	4.35	0.54	1.04	6.72 ± 0.18	**0.03**	0.03	8.5
0.6	9.02	1.21	2.42	14.84 ± 0.30	**0.08**	0.08	8.1
1	15.52	1.85	3.88	23.97 ± 0.31	**0.14**[b]	0.13	8.6
1.4	14.53	1.84	3.76	23.16 ± 0.28	**0.14**[a]	0.12	8.1
2	14.59	1.74	3.76	22.76 ± 0.18	**0.13**	0.14	8.5
2.6	17.68	2.19	4.55	27.92 ± 0.30	**0.17**	0.13	8.0
3	18.51	2.20	4.73	28.76 ± 0.26	**0.18**	0.15	8.6
3.4	20.64	2.40	5.39	32.06 ± 0.29	**0.21**	0.22	10.5
4	25.15	2.96	6.53	39.15 ± 0.33	**0.27**[b]	0.26	10.2
5	24.38	2.99	6.46	38.73 ± 0.14	**0.27**[a]	0.23	9.7
meta-MPYNNI	62.63	7.68	16.85	100	–	–	1.6

Superscripts a and b in table entries refer to two separate preparations resulting in samples with identical compositions.

[a] ESR line width.

Table 2
Chemical analysis data (ICP) of $Cd_{1-x}PS_3(meta\text{MPYNN})_{2x}$ samples.

Sample	mg/g ($\pm5\%$)			Elemental composition
	Cd	P	S	
$CdPS_3$	470	130	360	$Cd_1P_1S_{2.7}$
$x=0.13$	310	96	280	$Cd_{0.88}P_1S_{2.8}(meta\text{MPYNN})_{0.35}$
$x'=0.27$[b]	150	<30	76	$Cd_{1.58}P_1S_{2.8}(meta\text{MPYNN})_2I_{3.16}$

$x<0.20$. In contrast the Cd/P ratio of the high-intercalation regime sample disagrees with a sample composition of this formula. The deviation may be explained by the formation of a second reaction product. By intercalation of the radical and decomposition of the host lattice Cd^{2+} ions are released to the intercalation solution, which contains the radical cation and the iodide anion. For a highly concentrated solution, as present for the high-intercalation regime, the radical iodocadmate $CdI_4(meta\text{MPYNN})_2$ could be generated, according to the reaction:

$$CdI_2 + 2\ meta\text{-MPYNNI} \rightarrow CdI_4(meta\text{MPYNN})_2$$

Iodocadmates of this form are reported to be formed in highly concentrated solutions of CdI_2 with various alkylammonium compounds [34]. As discussed further below, additional evidence for the formation of this iodocadmate is provided by the XRD and ^{113}Cd MAS-NMR data. $CdI_4(meta\text{MPYNN})_2$ has 44 wt% of organic material and therefore its formation would agree with the observed elemental analysis data in the high-intercalation regime. The obtained ICP data in Table 2 are consistent with the formation of $CdI_4(meta\text{MPYNN})_2$ and $Cd_{1-x}PS_3(meta\text{MPYNN})_{2x}$ with $x=0.21$ in approximately equimolar proportions. While this x-value is associated with some uncertainty, further results, such as X-ray diffraction data or ^{31}P NMR measurements, argue in favor of an x larger than 0.14, which is observed for the low-intercalation regime. In spite of the above discussion, the sample compositions will be labeled in a formal way based on the assumption that all of the radical content has been intercalated and for the compositions of samples containing an iodocadmate impurity the notation x' will be used. To verify this hypothesis of a side reaction, the (previously not known) radical iodocadmate was prepared in a separate reaction from stoichiometric amounts of CdI_2 and *meta*-MPYNNI in methanol at 50 °C. Chemical analysis data (CHN) of this material were found in excellent agreement with the proposed elemental composition. As detailed further below, XRD and solid state NMR data clearly identify this material as a side product in intercalation reactions conducted at high R values. Finally, we have confirmed the structure of this material by single crystal X-ray diffraction (data to be published separately).

Table 1 summarizes the EPR linewidths of the intercalation compounds. In comparison to the pure radical iodide salt the g-value measured in the intercalation compounds remains unchanged at $g=2.006$. However, while solid *meta*-MPYNN iodide has a line width of 1.6 G, the line widths of the intercalation compounds are increased to 8.5 G and ~10 G in the low- and high-intercalation regimes, respectively. The two-stage behavior seen in the radical uptake curve is also seen in the dependence of the EPR linewidth on R (Fig. 2). Most likely, the transition observed near $x'=0.20$ reflects the contribution of the radical iodocadmate to the spectrum.

3.2. X-ray powder diffraction

Fig. 3 summarizes the X-ray powder diffraction data. The (001) reflection for pure $CdPS_3$ is observed at 13.6°, implying that the

slab center separation is 6.5 Å. For the concentration regime $0 \le x \le 0.14$, the diffraction patterns are superpositions of those observed for non-intercalated $CdPS_3$ and a set of new reflections with 2θ-values of 5.4°, 10.8° and 16.3°, which are assigned to the (001), (002) and (003) reflections of the intercalated material. The slab center separation amounts to 16.3 Å in this sample. In addition, samples with x near 0.13 show strong reflections at 7.1° and 14.2°, which corresponds to a slab center separation of 12.3 Å. These two reflections are absent at higher x-values. For the high-intercalation regime, the reflections at 2θ values near 5.4°, 10.8° and 16.3° are very sharp, suggesting a rather well-ordered structure. The many additional diffraction peaks originate neither from pure $CdPS_3$ nor from the potential contaminants CdI_2 or the radical cation iodide. Fig. 3 confirms that these peaks are clearly assignable to the iodocadmate CdI_4(*meta*MPYNN)$_2$.

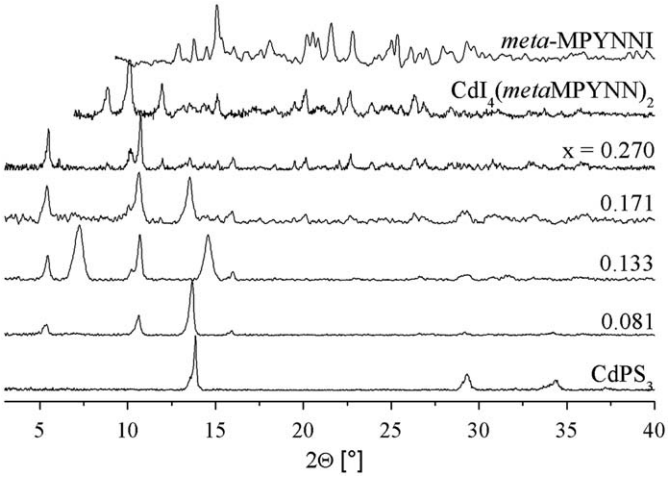

Fig. 3. Representative examples of powder X-ray pattern of the intercalation series of $Cd_{1-x}PS_3$(*meta*MPYNN)$_{2x}$ compared with those of pure $CdPS_3$, CdI_4(*meta*MPYNN)$_2$ and *meta*-MPYNNI.

In principle, the extent of the interlayer expansion contains information about the orientation of the guest species relative to the layered slabs. As illustrated by Fig. 4a the molecular dimensions of the radical cation *meta*-MPYNN$^+$ are 4.6, 5.8 and 9.8 Å. Therefore, three simple intercalation scenarios are imaginable (see Fig. 4b). If the radical is intercalated in a "flat" way with respect to the layers, the slab separation would increase from 6.5 to 11.1 Å. "Transversal" intercalation perpendicular to this direction with the N–O director pointing towards the layers would produce an expansion of 12.3 Å, while "longitudinal" intercalation with the NO bonds nearly parallel to the layers and pointing towards each other should result in a layer distance of 16.3 Å. While there are of course many other in-between possibilities, it turns out that the diffraction data can be satisfactorily explained on the basis of these three simple scenarios. While the intercalation compound with the longitudinal orientation of the guest species appears to be present at all the compositions studied, materials with $x \sim 0.13$ contain a significant contribution from the transversal intercalation compound as well. In contrast, the flat orientation is never observed. For the

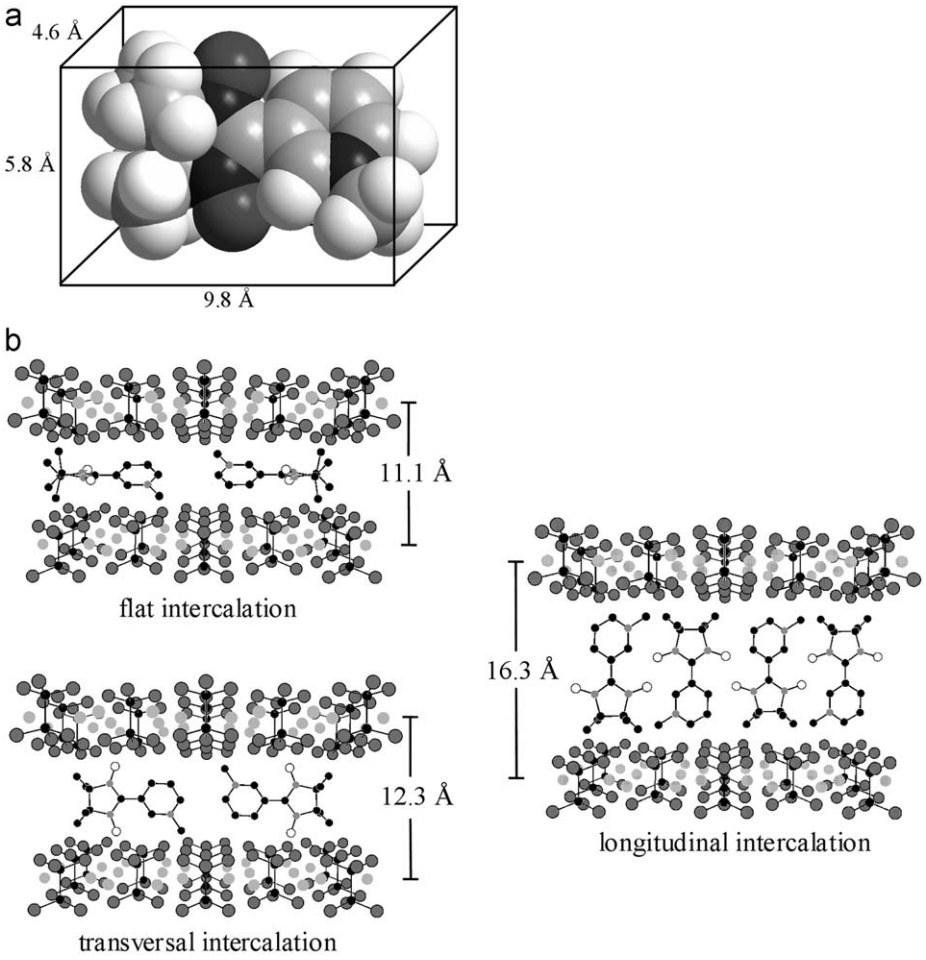

Fig. 4. (a) Dimensions of *meta*-MPYNN. (b) Schematic descriptions of three possible intercalation scenarios of *meta*-MPYNN into layered $CdPS_3$.

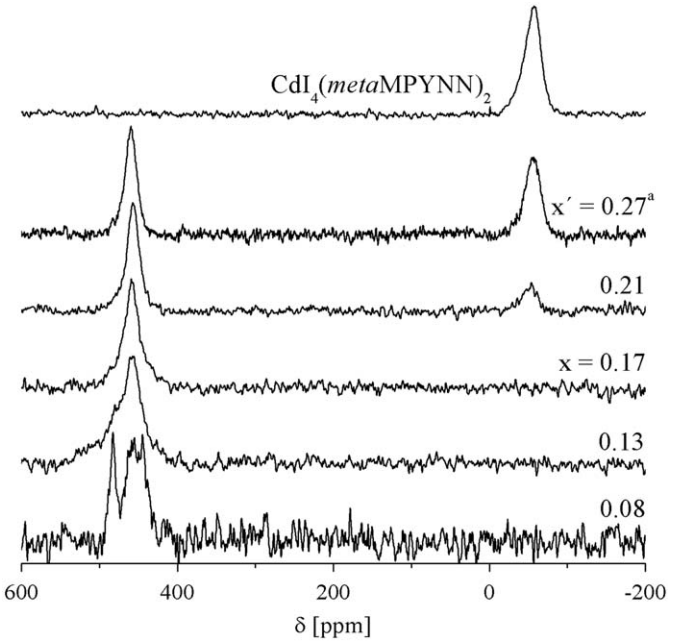

Fig. 5. ^{113}Cd MAS NMR spectra of $Cd_{1-x}PS_3$(*meta*MPYNN)$_{2x}$ intercalates and CdI_4(*meta*MPYNN)$_2$.

high-intercalation regime ($x' \geq 0.21$) the longitudinal orientation appears to be dominant.

3.3. ^{113}Cd NMR results

Fig. 5 summarizes the ^{113}Cd NMR data. The spectrum of the x=0.08 sample shows a narrow contribution at 482 ppm assigned to residual unintercalated host material [17], while the broad signal near 453 ppm reflects the structural perturbations experienced by Cd atoms owing to the intercalation process. Both signals are also characterized by very different spin-lattice relaxation behaviors. While the 482 ppm signal is characterized by T_1 values on the order of several minutes, $T_1 < 1$ s for the signal at 453 ppm. For the x=0.13 sample, only the latter resonance is observed near 457 ppm. The asymmetric structure of this peak may reflect several partially resolved components. This suggests that the host lattice at this intercalation degree is not well-ordered at this point, which confirms the structural discussion above (presence of both transversal and longitudinal intercalation). The spectrum for the sample with x=0.17 shows only one signal at 459 ppm. With increasing x this signal becomes narrower and better defined, indicating an increase in ordering with increasing x. For $x' \geq 0.21$ an additional peak at -56 ppm appears, which originates from CdI_4(*meta*MPYNN)$_2$. We attribute the large chemical shift change relative to that of pure CdI_2 (-713 ppm [35]) to the strong interaction of the ^{113}Cd nuclei with the unpaired electrons. For the sample with x'=0.27 the ratio between the two signals is 1:1. This verifies the suggestion above that this sample is composed of roughly equimolar proportions of iodocadmate and intercalated sample with $x \sim 0.2$. Also the signal area ratio of 4:1 in the spectrum of the x'=0.21 sample is consistent with a maximum intercalation degree of $x \sim 0.2$.

3.4. Magnetic properties

Fig. 6 summarizes the magnetic susceptibility data of two intercalated samples and compares them with the magnetic behavior of the pure salt. By fitting the data with a Curie–Weiss law a mass dependent Curie constant C_g and a Weiss temperature θ can

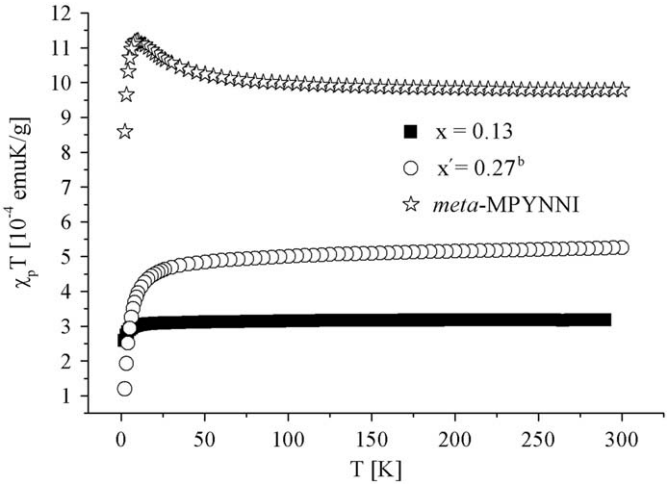

Fig. 6. Comparison of $\chi_p T$ data as a function of temperature of two different $Cd_{1-x}PS_3$(*meta*MPYNN)$_{2x}$ intercalates and the radical ion salt *meta*-MPYNNI.

Table 3
Weiss temperature θ, mass dependent Curie constant C_g and radical contents x or x' determined by different methods for three intercalation compounds $Cd_{1-x}PS_3$ (*meta*MPYNN)$_{2x}$.

	θ (K)	C_g (10^{-4} emu K/g)	x determined by		
			SQUID	CHN	EPR
x=0.13	−0.3	3.14	0.120	0.133	0.137
x'=0.27[a]	−4.0	5.27	0.231	0.266	0.231
x'=0.27[b]	−3.7	5.72	0.259	0.270	0.261
meta-MPYNNI	−2.9	9.62	–	–	–

be obtained (see Table 3). Approximating the intercalated organic radicals as single spins, which behave Curie-like with a Curie constant C of 0.375 emuK/mol, the magnetic susceptibility data afford an independent determination of the x- (and x') values. As summarized in Table 3 these x-values are in good agreement with those obtained via elemental analysis and EPR spectroscopy. A detailed inspection of the susceptibility curves reveals important differences for the two concentration regimes: for $x \leq 0.14$ Curie-like behavior with a Weiss temperature close to 0 K is observed, indicating that the radical species are essentially isolated from each other. This situation resembles that previously observed for radical ion intercalation into saponite [18,19] and into layered double hydroxide and zirconium phosphate hosts [17]. In contrast significant antiferromagnetic interactions are observed for the x'=0.27 samples, with the Weiss constant θ near -4 K. The strong antiferromagnetic behavior suggests a defined radical intermolecular arrangement, but this arrangement is apparently different from that in the pure radical ion salt, where an additional ferromagnetic contribution is observed. At the present stage, the interpretation of the magnetic data in the high-intercalation regime remains tentative, however, because they are also influenced by the additional iodocadmate present in these samples.

3.5. ^{1}H Solid state NMR

Fig. 7 summarizes the ^{1}H solid state NMR data at room temperature. Numerous signals corresponding to chemically non-equivalent protons of the nitroxide guest species are observed, indicating that the intercalation process can be monitored by

high-speed ^{1}H MAS NMR spectra. Table 4 summarizes the chemical shifts observed and the corresponding assignments. Compared to the pure radical iodide salt, the chemical shift values are significantly altered, particularly at low *x*-values, suggesting that the molecular spin density within the radical ions is dramatically changed upon intercalation. Spectra of samples in the high-intercalation regime ($x' \geq 0.21$) are dominated by the resonances of the iodocadmate impurity, which overlap those of the intercalate. Variable temperature measurements were conducted on three representative samples and are collected in Figure S-1 (Supplemental Material). The isotropic chemical shifts are dominated by the Fermi-contact interaction, as expressed by the relation [36],

$$\delta_{iso} \cong \frac{A_{Fermi}}{\gamma_i/2\pi} \frac{\chi_M}{N_A g \beta_e} + \delta_{dia}$$

and they are—because of their proportionality to the magnetic susceptibility χ_M—strongly temperature dependent. Thus, a plot of δ_{iso} vs. $1/T$ leads to the hyperfine coupling constants A_{Fermi} which in turn relates to the spin density $\rho(i)$ at the particular nucleus *i* observed according to

$$A_{Fermi} = \frac{8\pi}{3} g \beta_e \frac{\gamma_i}{2\pi} \rho(i)$$

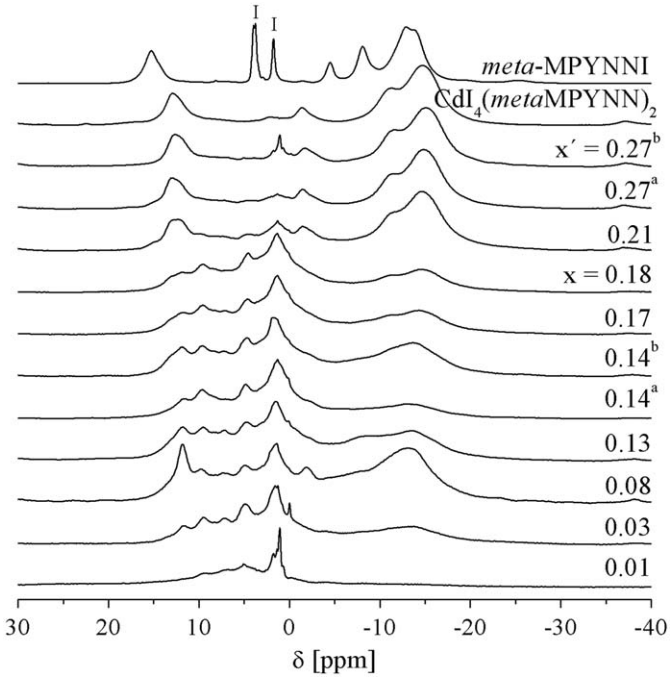

Fig. 7. ^{1}H-MAS-NMR spectra of $Cd_{1-x}PS_3$(*meta*MPYNN)$_{2x}$.

Here γ_i is the gyromagnetic ratio of the nuclear species considered and all other symbols have their usual meanings. Table 5 compares the coupling constants of the intercalates to those of the pure radical salt. Consistent with the magnetic susceptibility curves, the molecular spin distributions observed in the intercalated radical cations differ greatly from those measured in the pure radical cation iodides. The coupling constants corresponding to the aromatic moiety are smaller in the intercalate, while those for the *β*-methyl protons tend to be higher. This indicates that for the intercalation compound the unpaired electron density is more concentrated inside the nitronyl nitroxide moiety, possibly due to a larger torsion angle between this group and the aromatic ring. The higher spin density observed for the *β*-methyl groups might also explain the stronger pronounced antiferromagnetic interaction observed in the $x' = 0.27$ sample.

3.6. $^1H\{^{31}P\}$ REDOR

A better understanding of the radical arrangement and orientation in the interlayer space can be obtained by $^1H\{^{31}P\}$ REDOR experiments. The analysis of these measurements is only carried out for the *β*-methyl and *N*-methyl protons as only the latter show well-resolved signals that are clearly assignable in all the samples with different intercalation degrees. For the *β*-methyl group only data for very short dipolar evolution times can be measured as its signal decays very fast due to a very short T_2. As Fig. 8 illustrates, the *N*-methyl group shows a significantly stronger dephasing effect than the *β*-methyl group, at any composition *x*. The dependence of the M_2 ($^1H\{^{31}P\}$) value upon *x* is summarized in Fig. 8 (left). For the *N*-methyl group, the M_2 values remain more or less constant at $3.0–4.0 \times 10^6$ rad^2 s^{-2} within the stage-1 regime ($x \leq 0.13$). Assuming that the protons mainly interact with one closest ^{31}P neighbor, we can estimate the corresponding ^{1}H–^{31}P distance to 4.2 Å. This value is comparable to the P–P VAN-DER-WAALS distance in non-intercalated $CdPS_3$. Based on this comparison it can be concluded that these proton groups are in close contact with the layers. They are consistent with a Coulombic interaction model of these intercalates, where the positively charged nitrogen atom of the pyridinium unit is attracted by the negatively charged cadmium vacancy. Because of this specific interaction, the protons of the *N*-methyl group experience the strongest dipolar interactions with the ^{31}P host lattice nuclei.

For the stage-2 intercalates a significant decrease of M_2 values is observed. This effect can be attributed to the simultaneous presence of the radical iodocadmate, which—owing to the absence of ^{31}P nuclei—shows no REDOR effect. For example, at $x' = 0.27$ the M_2 measured for the *N*-methyl protons is only 20–25% of the M_2 measured at low *x*-values, suggesting that only

Table 4
Isotropic ^{1}H chemical shifts *δ*[ppm] of the different $Cd_{1-x}PS_3$(*meta*MPYNN)$_{2x}$ samples.

x	Aromatic	*β*-methyl	*N*-methyl	Unassigned
meta-MPYNNI	50.5; 44.9(2); -4.5	−8.1; −12.8(2); −14.2	15.3	–
0.03	–	−4; −8; −13.2	11.8	9.5; 7.2; 4.9; 1.6
0.08	−2	−5; −8; −13.2	11.8	9.4; 7.4; 4.9; 1.6
0.13	41–29	−8; −13.6	11.8	9.7; 7.2; 4.7; 1.5
0.14[a]	40–32	−13.1	11.2	9.6; 7.1; 4.8; 1.3
0.14[b]	37–28	−8; −11.4; −13.8	12.0	9.7; 7.2; 4.7; 1.6
0.17	–	−8.7; −11.4; −14.3	11.9	9.5; 7.2; 4.6; 1.3
0.18	–	−8.2; −11.1; −14.5	12.3	9.6; 4.6; 1.4
0.21	42; 34; 31; −1.6	−11.6; −14.7	12.4	4.5
0.27[a]	41; 34; 30.5; −2.0	−11.5; −14.9	12.6	–
0.27[b]	42;34; 31; −1.9	−11.7; −15.2	12.5	–

Table 5
Comparison of A_{Fermi} and diamagnetic shifts δ_{dia} of protons in *meta*-MPYNNI and $Cd_{1-x}PS_3$(*meta*MPYNN)$_{2x}$, as determined from fitting the temperature dependence of the isotropic ^{1}H MAS NMR shifts.

Proton site	*meta*-MPYNNI		$Cd_{1-x}PS_3$(*meta*MPYNN)$_{2x}$					
			x=0.08		x=0.13		x=0.27[b]	
	A_{Fermi} (±5%) (MHz)	δ_{dia} (±1) (ppm)	A_{Fermi} (±8%) (MHz)	δ_{dia} (±2) (ppm)	A_{Fermi} (±8%) (MHz)	δ_{dia} (±2) (ppm)	A_{Fermi} (±8%) (MHz)	δ_{dia} (±2) (ppm)
Aromatic	1.52	13.5						
	1.26	14.1					0.92	11.3
	−0.45	6.0	−0.33	4.6	−0.33	4.2	−0.39	7.3
N-methyl	0.29	8.3	0.23	6.2	0.23	6.3	0.19	7.9
β-methyl	−0.33	0.0						
	−0.49	−0.8	−0.60	3.0	−0.41	1.7	−0.55	2.5
	−0.56	−0.2	−0.67	3.6	−0.77	6.7	−0.72	3.7

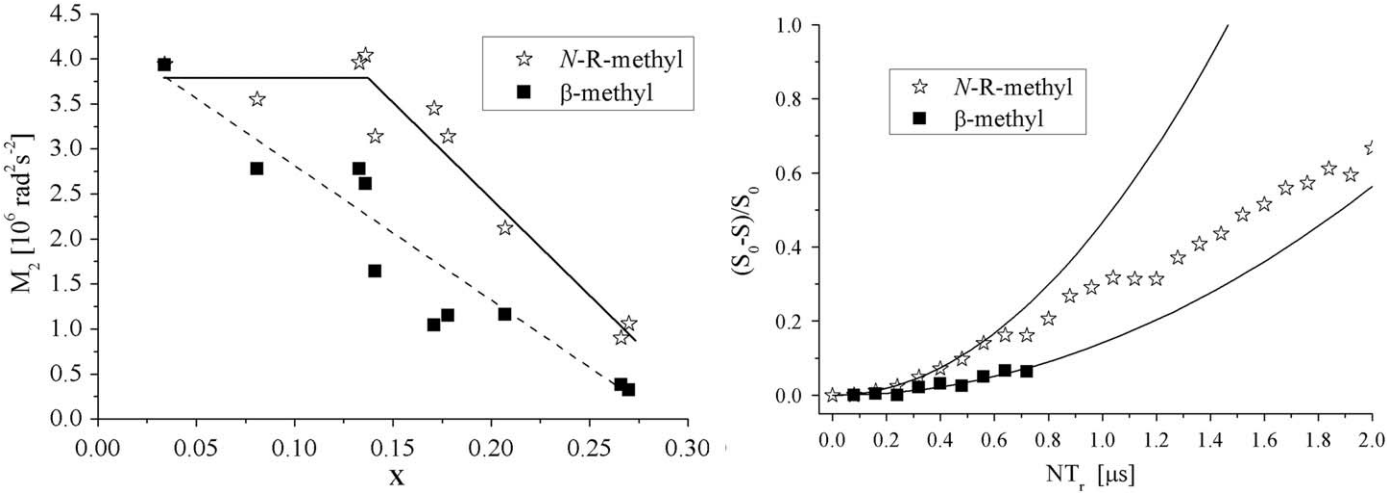

Fig. 8. Left: M_2 values of the *N*-R-methyl and *β*-methyl group of $Cd_{1-x}PS_3$(*meta*MPYNN)$_{2x}$ determined by ^{1}H{^{31}P} REDOR. Solid and dashed lines are guides to the eye. Abscissa values denote nominal compositions, which correspond to x in the low and x' in the high intercalation regimes. Right: Exemplary ^{1}H{^{31}P} REDOR curve with parabolic fits (solid curves) for the intercalate with x=0.17.

~20–25% of the total ^{1}H NMR signal arises from the radical inside the host lattice, while the remainder comes from the iodocadmate. This result is consistent with the previous conclusion from chemical analysis and ^{113}Cd NMR that in the x'=0.27 sample the iodocadmate and the inclusion compound with x~0.2 are present in roughly equimolar proportions.

In contrast to the *N*-methyl groups, the *β*-methyl groups show a weaker dipolar coupling to ^{31}P, and a monotonic decrease of M_2 as a function of x, suggesting that their interaction with the P atoms in the host layers is defined to a lesser degree than for the *N*-methyl group. This result can be rationalized as Coulombic forces are not involved in this case.

3.7. ^{31}P NMR results

The ^{31}P MAS NMR data are summarized in Fig. 9. As illustrated by the deconvolution shown for the x=0.14[b] sample (Fig. 10), three distinct contributions, with chemical shifts near 105, 103.4 and 101 ppm can be identified. Figure S-II (Supplemental Material) shows the compositional dependences of the peak positions and line widths. By comparison with the X-ray diffraction results and with the NMR spectrum of pure $CdPS_3$, the peak around 103.4 ppm must clearly be attributed to P atoms that are remote from the radical ions. The lineshape parameters of this peak show only little variations. These results allow no definite conclusion on

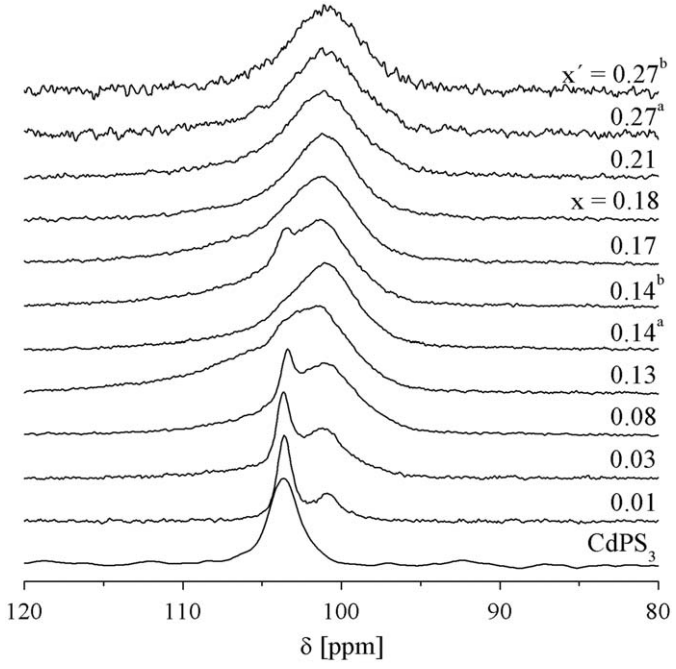

Fig. 9. ^{31}P MAS NMR spectra of $Cd_{1-x}PS_3$(*meta*MPYNN)$_{2x}$ intercalates and of $CdPS_3$, accumulated with a relaxation delay of 15 s.

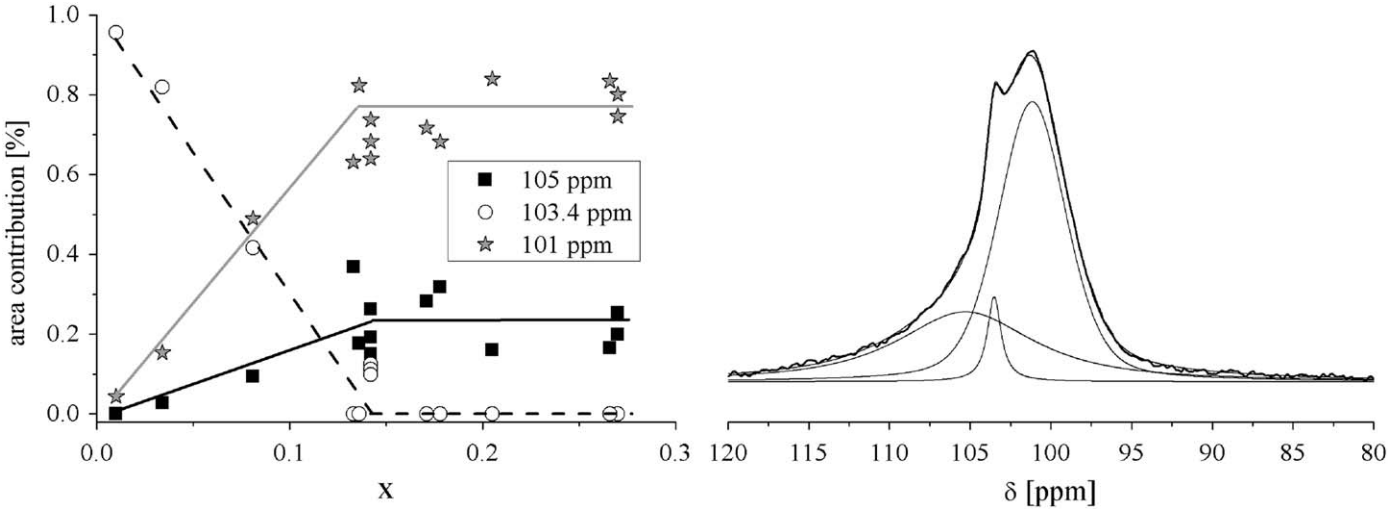

Fig. 10. Left: Area contributions of the three different peaks in the ^{31}P MAS NMR spectra of $Cd_{1-x}PS_3$(*meta*MPYNN)$_{2x}$. Abscissa values denote nominal compositions, which correspond to x in the low and x' in the high intercalation regimes. Right: ^{31}P MAS NMR spectrum and fit of intercalate with $x=0.14^b$.

whether samples in the low-intercalation regime are bi-phasic, consisting of unaltered $CdPS_3$ and fully intercalated material or whether they are single-phase with a distribution of local environments. As discussed further below, this question can be resolved on the basis of spin-lattice relaxation time and $^{31}P\{^1H\}$ REDOR measurements. As expected the 103.4 ppm signal contribution to the whole spectrum decreases linearly with increasing x and finally vanishes near $x=0.13$. In contrast, the lineshape contributions around 105 and 101 ppm increase with increasing x in this range, signifying P atoms in proximity to the intercalated species. The area ratio A(105 ppm)/A(101 ppm) remains essentially constant at 1:3 over the entire series. In those samples for which the X-ray data indicate the presence of substantial contributions of the transversal intercalation compound ($x=0.13$, $x=0.14^b$) the peak near 105 ppm appears to be somewhat better defined than in the other samples and seems to make a stronger contribution to the spectra.

The magnetization build-up curves measured during saturation recovery (Fig. 11a) show that the three ^{31}P spectral components identified above are distinguished by rather different spin-lattice relaxation behaviors. The 105 ppm lineshape component shows extremely fast relaxation ($T_1 \sim 50$ ms), signifying strong interactions of the corresponding ^{31}P nuclei with unpaired spin density. Based on this relaxation behavior, this resonance is assigned to phosphorus atoms in closest proximity to the unpaired electrons. The phosphorus species giving rise to the 101 and 103.4 ppm signals show slower relaxation behavior, and their rates depend systematically on the composition. Most interestingly, Fig. 11b shows that the P atoms contributing to the 101 ppm peak are characterized by bimodal relaxation behavior, i.e. the resonance most likely consists of two separate contributions, which can be distinguished by a two-orders-of-magnitude difference in T_1 (150 ms and 5 s, respectively). The fraction of the fast-relaxing contribution increases with increasing x. Based on this observation, the fast relaxing part is attributed to ^{31}P atoms in proximity to the unpaired electron (yet in a different environment than the P atoms contributing to the 105 ppm signal), whereas the slowly relaxing part is assigned to ^{31}P nuclei that are not close to unpaired spin density. For the fully intercalated sample ($x'=0.27$), only the fast relaxing part is observed, and its relaxation behavior is no longer clearly distinguishable from that observed at 105 ppm. The relaxation times of the signals near 105 ppm increase gradually with x, while the relaxation times of the fast

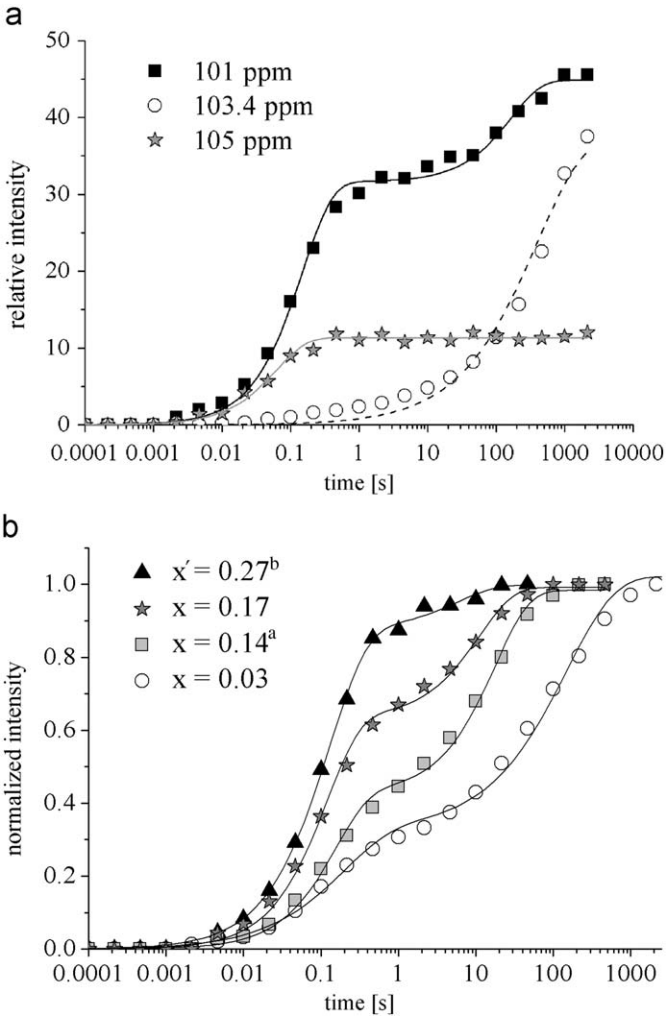

Fig. 11. (a) Magnetization build-up curves for the three identified ^{31}P species in $Cd_{1-x}PS_3$(*meta*MPYNN)$_{2x}$ ($x=0.08$). (b) Bimodal magnetization build up curves of the ^{31}P signal at 101 ppm for different compositions.

relaxing part of the 101 ppm peak decrease (see Figure S-III, Supplemental Material). Finally, the 103.4 ppm resonance observed for compositions $x \leq 0.14$ is characterized by T_1 values

close to that of the non-intercalated $CdPS_3$, but decreasing systematically with increasing radical cation content. This noticeable influence of x upon the relaxation behavior of those phosphorus atoms suggests that samples in the stage-1 regime ($x < 0.14$) are not macroscopically phase separated into pure $CdPS_3$ and fully intercalated material. Rather, those P atoms contributing to the 103.4 ppm resonance most likely originate from sample regions that are remote from radical ions, but still in contact with faster relaxing regions. As will be discussed below, this conclusion is reinforced by the $^{31}P\{^1H\}$ REDOR data.

3.8. $^{31}P\{^1H\}$ double resonance NMR

To further aid the assignment of the various ^{31}P resonances observed in the ^{31}P MAS NMR spectra $^{31}P\{^1H\}$ REDOR experiments were carried out. Fig. 12, which shows the results obtained for the $x=0.03$ sample, clearly illustrates the power of this experiment in differentiating the three distinct phosphorus species. The strongest dipolar dephasing is observed for the signal at 101 ppm, indicating that these ^{31}P species are in closest proximity to the guest species' protons. By comparison the 105 ppm component shows somewhat weaker dipolar couplings. For higher x-values the dipolar interaction strengths converge suggesting similar ^1H–^{31}P dipolar coupling strengths. Finally, the REDOR data measured for the 103.4 ppm peak signify weak, yet non-zero magnetic dipole–dipole couplings with ^1H nuclei, the strengths of which increase with increasing x. This result supports the previous conclusion from the relaxation time measurements about the single-phase character of these materials.

The strong and almost compositionally independent ^1H–^{31}P magnetic dipole–dipole coupling observed for the 101 ppm peak indicates that this P species has a well-defined proton environment resulting from local energy constraints rather than from distance statistics. Consistent with the conclusions from $^1H\{^{31}P\}$ REDOR this signal is attributed to P atoms close to the (negatively charged) Cd^{2+} vacancy which should attract the positive charge center of the radical ion. Based on this idea, the protons associated with the N-methyl group of the pyridyl moiety should experience particularly strong magnetic dipole–dipole interactions with the ^{31}P nuclei of the host lattice as shown in the $^1H\{^{31}P\}$ REDOR experiments. This idea is tested further by $^{31}P\{^1H\}$ heteronuclear correlation experiments. Fig. 13 summarizes these results for the $x=0.14^b$ and $x'=0.27^a$ samples. While the single pulse ^{31}P spectrum of the sample with $x=0.14^b$ has contributions of the signals at 103.4 and 105 ppm, these contributions are absent in the $^{31}P\{^1H\}$ CPMAS NMR spectra. This is expected for the signal at 103.4 ppm, which is due to P atoms remote from guest species and which also shows only a weak REDOR effect, and therefore should not appear in the cross-polarization spectrum. That the signal at 105 ppm is also almost absent can be attributed to the strong paramagnetic interactions these P atoms are exposed to. The only clearly observable correlation peaks are between the signal at 101 ppm (^{31}P) and the signals of the N-methyl protons and the β-methyl protons, where the N-methyl contribution is significantly enhanced. Also the so far unassigned ^1H NMR signal near 1.6 ppm shows a strong correlation with ^{31}P and must therefore also belong to a proton species on the intercalated radicals. The $^{31}P\{^1H\}$ HETCOR spectrum of the $x'=0.27^a$ inclusion compound shows mainly the same results for the signal at 101 ppm. Owing to the slightly longer relaxation times associated with the 105 ppm ^{31}P signal component a correlation peak involving this resonance is visible in this case. The observed correlation peak between this signal and the signal arising from the β-methyl group confirms the above made suggestion that the phosphorus sites at 105 ppm are close to the paramagnetic center of the radical, the nitronyl moiety. Again the peak at 101 ppm shows the strongest correlation with the unassigned signals and the N-methyl signal, whereas the correlation of the β-methyl protons is somewhat weaker. These observations are consistent with the assignment of the 101 ppm site to those P atoms in the lattice that are near a Cd vacancy (and thus close to the positively charged center of the radical ion). Finally, we point out that the indirectly (via CPMAS) detected spectrum along the ^1H dimension only arises from protons in the intercalate that are in close contact with ^{31}P, whereas the directly detected ^1H MAS-NMR spectrum represents the entire proton inventory (intercalate and iodocadmate) of the sample. Fig. 13 indicates that both spectra closely resemble each other. As the signal of the iodocadmate dominates the ^1H MAS-NMR spectra of samples with $x' \geq 0.21$, the HETCOR method affords a convenient method for the selective detection of the protons in the $CdPS_3$ intercalate.

3.9. ^{31}P J-Resolved NMR

Fig. 14 shows ^{31}P J-Resolved spectra of the low- and high-intercalated regime, respectively. The right sides of each figure show slices for the different observed phosphorus sites. For the sample with $x=0.14^b$ all three phosphorus environments

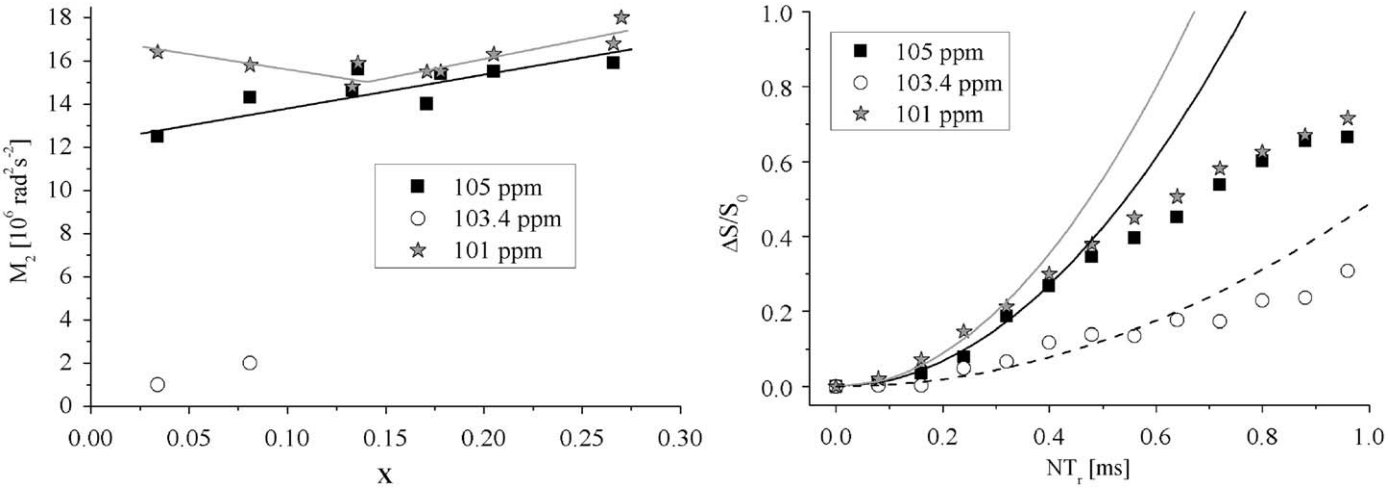

Fig. 12. Left: M_2 values of the three different ^{31}P sites of $Cd_{1-x}PS_3$(*meta*MPYNN)$_{2x}$. Abscissa values denote nominal compositions, which correspond to x in the low and x' in the high intercalation regimes. Right: Exemplary $^{31}P\{^1H\}$ REDOR curve with parabolic fits for the intercalate with $x=0.03$.

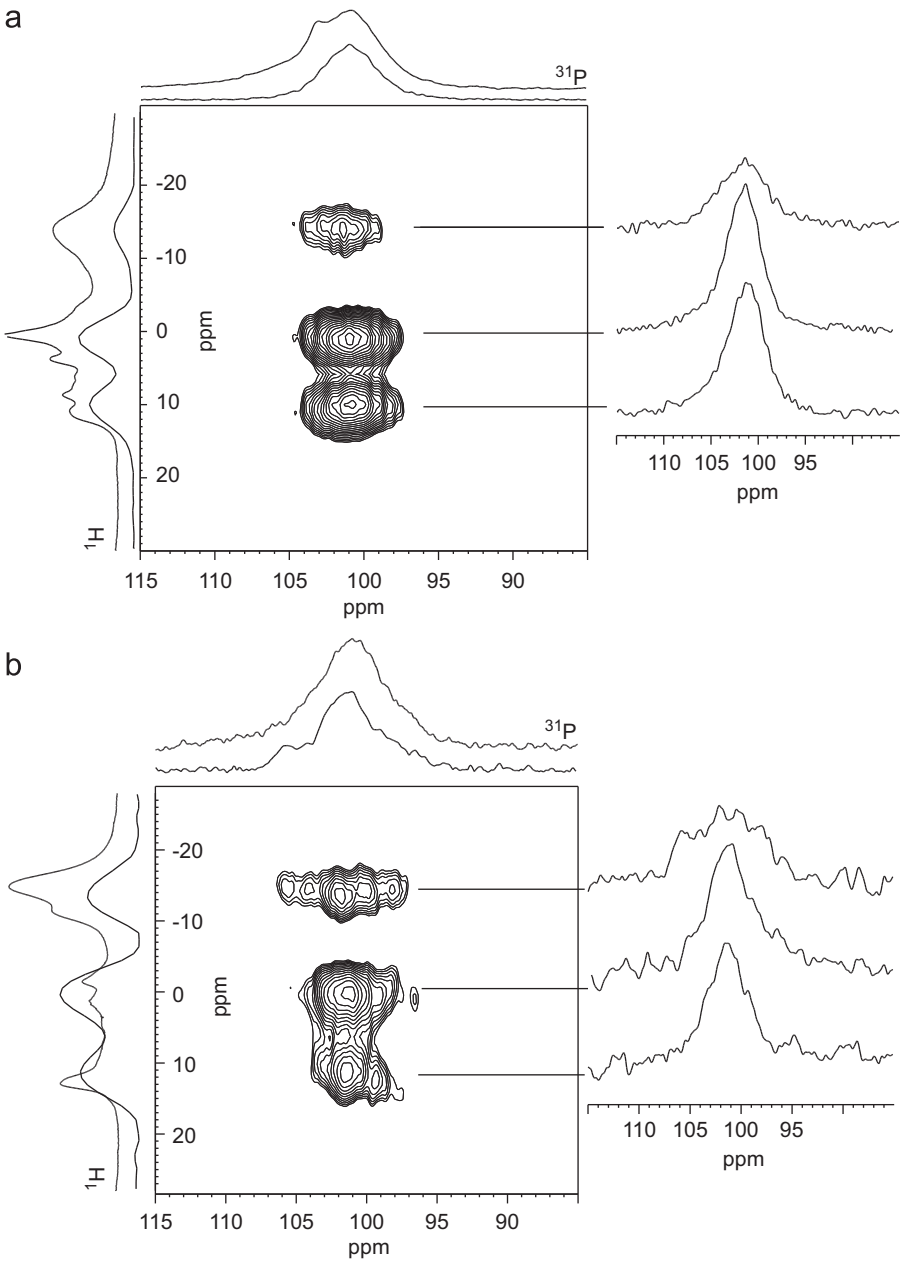

Fig. 13. (a) $^{31}P\{^{1}H\}$ HETCOR experiment of $Cd_{1-x}PS_3$(*meta*MPYNN)$_{2x}$ with $x=0.14^{b}$. The projections of the 2D plots onto the F1 and F2 dimensions are compared with the one pulse ^{1}H and ^{31}P MAS NMR spectrum, respectively. The right side shows ^{31}P slices for different proton shifts. (b) $^{31}P\{^{1}H\}$ HETCOR experiment of $Cd_{1-x}PS_3$(*meta*MPYNN)$_{2x}$ with $x'=0.27$. The projections of the 2D plots on the F1 and F2 dimensions are compared with the one pulse ^{1}H and ^{31}P MAS NMR spectrum, respectively. The right side shows ^{31}P slices for different proton shifts.

discussed above are present. The slice for the signal at 103.4 ppm shows a dominant singlet. The observed doublet contribution is attributed mainly to the partial overlap with the signals at 101 and 105 ppm. At 105 ppm only a doublet can be observed, indicating that the P atoms contributing to this resonance belong to $P_2S_6^{4-}$ groups in which the two P atoms are magnetically inequivalent. The most interesting observation in Fig. 14 is the fact that the slice at 101 ppm contains both a singlet and a doublet. Therefore, we conclude that these $P_2S_6^{4-}$ units consist on the one hand of two equal P atoms (singlet) and on the other hand of one P atom with a chemical shift 101 ppm and another one having a different shift. The doublet could be attributed to the fast relaxing fraction of this signal, where the $P_2S_6^{4-}$ units have on one side phosphorus close to the aromatic moiety (101 ppm) and on the other side a P atom close to the nitronyl moiety (105 ppm). This would also explain why these P atoms are relaxing faster than usual. The singlet would then be arising from $P_2S_6^{4-}$ units close to *N*-CH_3 groups on both sides of the layer. This arrangement preserves the center of inversion of these units leaving both P atoms magnetically equivalent. For the inclusion compound with $x'=0.27$, such a species is not clearly visible, which may be related to the smaller fraction of the slow-relaxing component contributing to the 101 ppm signal. The *J* coupling constant for all the doublets is 265 Hz and does not change with *x*.

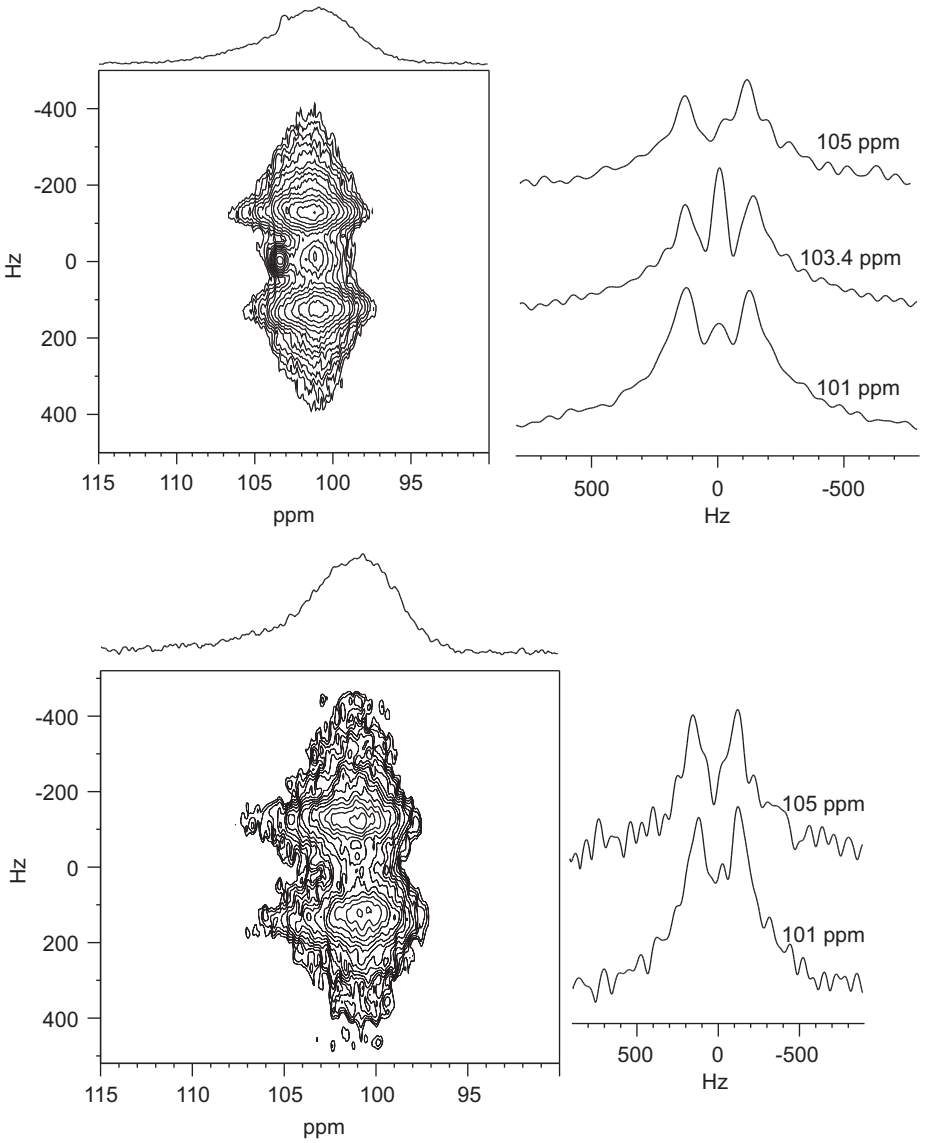

Fig. 14. (a) ^{31}P J-resolved experiment of $Cd_{1-x}PS_3$(*meta*MPYNN)$_{2x}$ with x=0.14. The right side shows ^{31}P slices for the chemical shift of the three phosphorus sites. (b) ^{31}P J-resolved experiment of $Cd_{1-x}PS_3$(*meta*MPYNN)$_{2x}$ with x'=0.27. The right side shows ^{31}P slices for the chemical shift of the three phosphorus sites.

4. Conclusions

In summary the results of the present study reveal important structural details concerning the intercalation of *meta*-MPYNN into $CdPS_3$. Radical uptake as a function of R shows a two-stage behavior with x near 0.13 and 0.20, for the first and the second stage, respectively. The first-stage intercalates show the simultaneous occurrence of transversal and longitudinal guest species orientations, whereas the second-stage intercalates are dominated by the longitudinal orientation. The second-stage intercalation is also accompanied by a side reaction leading to the precipitation of a radical iodocadmate CdI_4(*meta*MPYNN)$_2$. ^{1}H MAS-NMR spectra reveal substantial differences of the unpaired electron spin density distributions within the radical ions intercalated into the host lattice compared to those obtained for the pure radical ion salts, and also a significant difference in the intermolecular guest–guest interaction strengths, between first-stage and second-stage materials, leading to different bulk magnetic properties.

The NMR spectra of the host lattice nuclei ^{31}P and ^{113}Cd are well-suited to monitor the intercalation process and to follow the concomitant structural perturbations in the host lattice upon radical insertion. Intercalation of the radical ion produces a new ^{31}P signal near 101 ppm, reflecting P atoms in direct proximity to a negatively charged Cd vacancy. That these P atoms have the expected close distance to protons near the positive charge of the radical ion is confirmed by large M_2 values obtained for ^{31}P{^{1}H} REDOR experiments and by the intense cross-peaks in the ^{31}P{^{1}H} HETCOR spectra. Overall, the present study reveals the power and utility of advanced solid state NMR techniques for the structural characterization of organic radical intercalation materials.

Further studies reveal that *meta*-MPYNN is only one member of a whole family of nitroxide radical ions that can be intercalated successfully into $CdPS_3$. A whole variety of different magnetic behaviors can be generated for these materials, which can be discussed in the context of structural information on the molecular level provided by solid state NMR data. These results will be described in a subsequent publication.

Acknowledgments

W.L. Hemme would like thank the IRTG "Complex Functional Systems" (WWU Münster–Nagoya University) and the Fonds der Chemischen Industrie for a personal fellowship. Further financial support for this work from the IRTG Münster–Nagoya is most gratefully acknowledged.

Appendix A. Supplementary material

Supplementary data associated with this article can be found in the online version at doi:10.1016/j.jssc.2009.09.030.

References

[1] P.M. Allemand, K.C. Khemani, A. Koch, F. Wudl, K. Holczer, S. Donovan, G. Grüner, J.D. Thompson, Science 253 (1991) 301.
[2] M. Tamura, Y. Nakazawa, D. Shiomi, K. Nozawa, Y. Hosokoshi, M. Ishikawa, M. Takahashi, M. Kinoshita, Chem. Phys. Lett. 186 (1991) 401.
[3] Y. Hosokoshi, M. Tamura, H. Sawa, R. Kato, M. Kinoshita, J. Mater. Chem. 5 (1995) 41.
[4] M. Deumal, J. Cirujheda, J. Veciana, J. Novoa, Chem. Eur. J. 5 (1999) 1631.
[5] J. Veciana, J. Cirujeda, C. Rovira, J. Vidal-Gancedo, Adv. Mater. 7 (1995) 221.
[6] T. Kawakami, S. Yamanaka, W. Mori, Y. Yamaguchi, A. Kajiwara, M. Kamchi, Chem. Phys. Lett. 235 (1995) 414.
[7] K. Awaga, T. Inabe, Y. Maruyama, T. Nakamura, M. Matsumoto, Chem. Phys. Lett. 195 (1992) 21.
[8] K. Awaga, T. Inabe, Y. Maruyama, T. Nakamura, M. Matsumoto, Synth. Met. 55–57 (1993) 3311.
[9] B. Gillon, M.A. Aebersold, O. Kahn, L. Pardi, B. Delley, Chem. Phys. 250 (1999) 23.
[10] D.A. Souza, A.S. Florencio, J.W.D.M. Carneiro, S.S. Soriano, C.B. Pinheiro, M.A. Novak, M.G.F. Vaz, Inorg. Chim. Acta 361 (2008) 4024.
[11] S.P. Wang, J. Chen, D.Z. Gao, Y. Song, Q.M. Wang, D.Z. Liao, Z.H. Jiang, S.P. Yan, J. Coord. Chem. 58 (2005) 1695.
[12] I. Dasna, S. Golhen, L. Ouahab, N. Daro, J.P. Sutter, Polyhedron 20 (2001) 1371.
[13] N. Crivillers, M. Mas-Torrent, S. Perruchas, N. Roques, J. Vidal-Gancedo, J. Veciana, C. Rovira, L. Basabe-Desmonts, B.J. Ravoo, M. Crego-Calama, D.N. Reinhoudt, Angew. Chem. Int. Ed. 46 (2007) 2215.
[14] M. Mas-Torrent, N. Crivillers, I. Ratera, C. Rovira, J. Veciana, J. Mater. Chem. 19 (2009) 1691.
[15] O. Shekhah, N. Roques, V. Mugnaini, C. Munuera, C. Ocal, J. Veciana, C. Woell, Langmuir 24 (2008) 6640.
[16] N. Roques, D. Maspoch, A. Datcu, K. Wurst, D. Ruiz-Molina, C. Rovira, J. Veciana, Polyhedron 26 (2007) 1934.
[17] A. Caneschi, D. Gatteschi, C. Sangregorio, M.G.F. Vaz, U. Constantino, M. Nocchetti, R. Vivani, Inorg. Chim. Acta 338 (2002) 127.
[18] W. Fujita, K. Awaga, J. Chem. Soc. Chem. Commun. (1995) 739.
[19] W.L. Hemme, W. Fujita, K. Awaga, H. Eckert, J. Chem. Soc. Dalton Trans. (2009) 7995.
[20] R. Brec, Solid State Ionics 22 (1986) 3.
[21] S. Béenard, A. Léaustic, E. Rivière, P. Yu, R. Clément, Chem. Mater. 13 (2001) 3709.
[22] J. Schmedt auf der Günne, H. Eckert, A. Léaustic, F. Babonneau, Phys. Chem. Chem. Phys. 5 (2003) 1306.
[23] C.N. Field, M.-L. Boillot, R. Clément, J. Mater. Chem. 8 (1998) 283.
[24] S. Floquet, M.C. Munoz, E. Rivière, R. Clément, J.-P. Audière, M.-L. Boillot, N. J. Chem. 28 (2004) 535.
[25] E.F. Ullmann, J.H. Osiecki, D.G.B. Boocok, R. Darcy, J. Am. Chem. Soc. 94 (1972) 7049.
[26] K. Awaga, T. Inabe, U. Nagashima, T. Nakamura, M. Matsumoto, Y. Maruyama, Chem. Lett. (1991) 1777.
[27] T. Takahashi, H. Kawashima, H. Sugisawa, T. Baba, Solid State Nucl. Magn. Reson. 15 (1999) 119.
[28] D. Massiot, F. Fayon, M. Capron, I. King, S. Le Calve, B. Alonso, J.O. Durand, B. Bujoli, Z. Gan, G. Hoatson, Magn. Reson. Chem. 40 (2002) 70.
[29] L. Duma, W.C. Lai, M. Caravetta, L. Emsley, S.P. Brown, Chem. Phys. Chem. 5 (2004) 815.
[30] F. Fayon, I.J. King, R.K. Harris, J.S.O. Evans, D. Massiot, C.R. Chim. 7 (2004) 351.
[31] T. Gullion, J. Schaefer, J. Magn. Reson. 81 (1989) 196.
[32] M. Bertmer, H. Eckert, Solid State Nucl. Magn. Reson. 15 (1999) 139.
[33] J.C.C. Chan, H. Eckert, J. Magn. Reson. 147 (2000) 170.
[34] S.D. Ross, I.W. Siddiqi, H.J.V. Tyrrell, J. Chem. Soc. Dalton Trans. 15 (1972) 1611.
[35] S. Sakida, Y. Kawamoto, J. Phys. Chem. Solids 63 (2002) 151.
[36] G. Maruta, S. Takeda, A. Yamaguchi, T. Okuno, K. Awaga, Polyhedron 22 (2003) 1989.